Nonlinear Phenomena in Thermoacoustic Systems With Premixed Flames

Karthik Kashinath[1]
Engineering Department,
University of Cambridge,
Cambridge CB2 1PZ, UK
e-mail: kk377@cam.ac.uk

Santosh Hemchandra[2]
Institute of Aerodynamics,
RWTH Aachen University,
Aachen 52062, Germany
e-mail: s.hemchandra@aia.rwth-aachen.de

Matthew P. Juniper
Engineering Department,
University of Cambridge,
Cambridge CB2 1PZ, UK
e-mail: mpj1001@cam.ac.uk

Nonlinear analysis of thermoacoustic instability is essential for the prediction of the frequencies, amplitudes, and stability of limit cycles. Limit cycles in thermoacoustic systems are reached when the energy input from driving processes and energy losses from damping processes balance each other over a cycle of the oscillation. In this paper, an integral relation for the rate of change of energy of a thermoacoustic system is derived. This relation is analogous to the well-known Rayleigh criterion in thermoacoustics, however, it can be used to calculate the amplitudes of limit cycles and their stability. The relation is applied to a thermoacoustic system of a ducted slot-stabilized 2-D premixed flame. The flame is modeled using a nonlinear kinematic model based on the G-equation, while the acoustics of planar waves in the tube are governed by linearized momentum and energy equations. Using open-loop forced simulations, the flame describing function (FDF) is calculated. The gain and phase information from the FDF is used with the integral relation to construct a cyclic integral rate of change of energy (CIRCE) diagram that indicates the amplitude and stability of limit cycles. This diagram is also used to identify the types of bifurcation the system exhibits and to find the minimum amplitude of excitation needed to reach a stable limit cycle from another linearly stable state for single-mode thermoacoustic systems. Furthermore, this diagram shows precisely how the choice of velocity model and the amplitude-dependence of the gain and the phase of the FDF influence the nonlinear dynamics of the system. Time domain simulations of the coupled thermoacoustic system are performed with a Galerkin discretization for acoustic pressure and velocity. Limit cycle calculations using a single mode, along with twenty modes, are compared against predictions from the CIRCE diagram. For the single mode system, the time domain calculations agree well with the frequency domain predictions. The heat release rate is highly nonlinear but, because there is only a single acoustic mode, this does not affect the limit cycle amplitude. For the twenty-mode system, however, the higher harmonics of the heat release rate and acoustic velocity interact, resulting in a larger limit cycle amplitude. Multimode simulations show that, in some situations, the contribution from higher harmonics to the nonlinear dynamics can be significant and must be considered for an accurate and comprehensive analysis of thermoacoustic systems. [DOI: 10.1115/1.4023305]

1 Introduction

Lean premixed combustion systems are susceptible to thermoacoustic instabilities, which occur due to the interaction between the unsteady heat release rate and acoustic waves inside the combustor [1]. Linear stability analysis of such systems can be used to predict frequencies and growth rates of linearly unstable modes. However, they can predict neither limit cycle amplitudes, nor a system's susceptibility to oscillations triggered by finite amplitude excitations.

Several studies have investigated nonlinear phenomena in combustion instabilities. While early studies focused on nonlinear gas dynamics in solid-propellant rocket engines [2–6], later studies, especially those relevant to gas turbine combustors, explored the nonlinear behavior of the unsteady heat release rate [7–9]. Several nonlinear flame models relevant to gas turbine combustors have been proposed [10–15] based on theory and experiments. In recent years, complex nonlinear phenomena such as triggering, hysteresis, and mode-switching have been experimentally and numerically investigated [16,17].

The previously mentioned analyses use one of two types of approaches: time domain or frequency domain. It is useful to highlight the underlying assumptions in each method. In the frequency domain approach based on the (sinusoidal) flame describing function (FDF), one assumes that the fundamental frequency determines the dynamics of the system while higher harmonics generated in the nonlinear processes are of sufficiently low amplitude to have a negligible effect on the system's stability (Noiray et al. [16]). The FDF is then used in a nonlinear dispersion relation to calculate growth rates and frequencies as functions of the perturbation amplitude. Their analysis highlights the importance of the amplitude-dependence of the flame response delay on the nonlinear behavior of the system. While the frequency domain approach has been successful in some practical systems, Subramanian et al. [18] argue that the system behavior predicted using the FDF approach may be quantitatively and qualitatively different from that seen using time domain simulations of simple thermoacoustic models. They point out that using a two-part approach and a modal analysis fails to capture the intricate coupling between combustion and acoustics.

The aims of this paper are: (i) to examine the nonlinear thermoacoustic phenomena of a ducted premixed flame, and (ii) to evaluate the accuracy of limit cycle amplitudes calculated from the frequency domain against calculations from the time domain. An energy integral relation that assumes the existence of limit cycles is derived for a single mode thermoacoustic system. This integral relation is used with the FDF: (i) to calculate the

[1]Corresponding author.
[2]Present address: Department of Aerospace Engineering, Indian Institute of Science, Bangalore 560012, India.

Contributed by the International Gas Turbine Institute (IGTI) of ASME for publication in the JOURNAL OF ENGINEERING FOR GAS TURBINES AND POWER. Manuscript received September 18, 2012; final manuscript received November 30, 2012; published online May 20, 2013. Editor: David Wisler.

amplitudes and stability of limit cycles, (ii) to predict the types of bifurcation in such systems, and (iii) to estimate the minimum amplitude required to trigger a single-mode system into stable limit cycle oscillations. Time domain simulations are used to evaluate the accuracy of a particular case. Single-mode simulations show that the results obtained by applying the integral criterion along with the FDF are accurate, even when the nonlinearities in the heat release rate are not negligible. Multimode simulations, however, show that the higher harmonics contribute to the nonlinear dynamics and their impact can be significant in some situations. Although the thermoacoustic system under consideration in this paper is a simple ducted premixed flame, the fundamental nonlinear behavior observed here is relevant to more complex thermoacoustic systems because the main source of nonlinearity is captured well.

The rest of this paper is organized as follows. Sections 2 and 3 describe the models and governing equations for the acoustics and the flame, respectively. In Sec. 4, criteria for the amplitude and stability of limit cycles are derived. Section 5 describes the linear and nonlinear velocity-coupled heat release response of the flame and the influence of the choice of velocity model on them. In Sec. 6, diagrams that map the stability of thermoacoustic systems and the nonlinear phenomena observed in them are discussed. Section 7 shows simulations in the time domain and a comparison between the frequency and time domain calculations. Closing remarks with an outlook on future work are presented in Sec. 8.

2 Model for the Acoustics

For the sake of simplicity, the acoustic chamber in the thermoacoustic system considered here is a duct of length L_0, open at both ends with a slot-stabilized 2-D laminar premixed flame located at a distance $\tilde{x}_f$ from one end. Figure 1 shows a schematic illustration. The base flow velocity is $\tilde{u}_0$, the pressure is $\tilde{p}_0$, and a constant mean density assumption is invoked so that the mean density $\tilde{\rho}_0$ and the speed of sound in the unburnt mixture $\tilde{c}_0$ remain constant everywhere in the duct. The Mach number $M \equiv \tilde{u}_0/\tilde{c}_0$ is assumed to be small and, hence, nonlinear effects in the acoustics are negligible [11]. A compact flame assumption is used here because the flame length is small compared to the wavelengths of the duct's acoustic modes. The dimensional governing equations for the acoustic perturbations are the momentum and energy equations

$$\tilde{\rho}_0 \frac{\partial \tilde{u}}{\partial \tilde{t}} + \frac{\partial \tilde{p}}{\partial \tilde{x}} = 0 \tag{1}$$

$$\frac{\partial \tilde{p}}{\partial \tilde{t}} + \gamma \tilde{p}_0 \frac{\partial \tilde{u}}{\partial \tilde{x}} + \zeta \frac{\tilde{c}_0}{L_0} \tilde{p} - (\gamma - 1)\tilde{\dot{Q}}\delta(\tilde{x} - \tilde{x}_f) = 0 \tag{2}$$

where the rate of heat transfer from the flame to the gas is given by $\tilde{\dot{Q}}$, which is applied at the flame's position by multiplying $\tilde{\dot{Q}}$ by the dimensional Dirac delta distribution $\tilde{\delta}(\tilde{x} - \tilde{x}_f)$. The acoustic damping is represented by ζ and the model for this is described later.

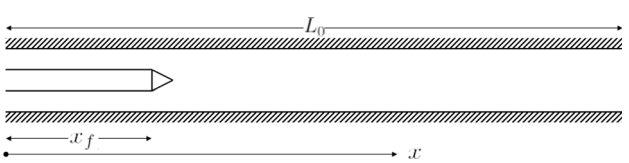

Fig. 1 Schematic of the two-dimensional slot stabilized premixed flame in a duct: L_0 is the length of the duct, $\tilde{x}_f$ is the flame position along the duct, $\alpha = 0.02$ is the fraction of the duct cross-sectional area occupied by the burner and the flow is from left to right

The preceding equations may be nondimensionalized using $\tilde{u}_0$, $\tilde{p}_0\gamma M$, L_0, and $L_0/\tilde{c}_0$ for speed, pressure, length, and time, respectively. The dimensionless governing equations are

$$\frac{\partial u}{\partial t} + \frac{\partial p}{\partial x} = 0 \tag{3}$$

$$\frac{\partial p}{\partial t} + \frac{\partial u}{\partial x} + \zeta p - \beta \dot{Q} \delta_D(x - x_f) = 0 \tag{4}$$

$$\beta \equiv \frac{(\gamma - 1)\tilde{\dot{Q}}_0 \alpha}{\gamma \tilde{p}_0 \tilde{u}_0}, \quad \dot{Q} \equiv \frac{\tilde{\dot{Q}}}{\tilde{\dot{Q}}_0} \tag{5}$$

where $\beta\dot{Q}$ is the nondimensional heat release rate perturbation, which encapsulates all relevant information about the flame, base velocity, and ambient conditions. The heat release rate is averaged over the cross-sectional area of the duct and the ratio of the area of the base of the flame to the cross-sectional area of the duct α is assumed to be 0.02 in this paper.

For the open duct examined here, the pressure perturbations and gradient of velocity perturbations are both set to zero at the ends of the tube

$$[p]_{x=0} = [p]_{x=1} = 0; \quad \left[\frac{\partial u}{\partial x}\right]_{x=0} = \left[\frac{\partial u}{\partial x}\right]_{x=1} = 0 \tag{6}$$

These boundary conditions are enforced by choosing basis sets that match these boundary conditions and satisfy the dimensionless momentum equation (Eq. (3)) as follows:

$$u(x,t) = \sum_{j=1}^{N} \eta_j(t)\cos(j\pi x); \quad p(x,t) = -\sum_{j=1}^{N} \frac{\dot{\eta}_j(t)}{j\pi}\sin(j\pi x) \tag{7}$$

In this Galerkin discretization, all of the basis vectors are orthogonal. The state of the system is given by the amplitudes of the Galerkin modes that represent the velocity η_j and those that represent the pressure $\dot{\eta}_j$. The energy equation is discretized by substituting Eq. (7) into Eq. (4). The acoustic damping ζ is dealt with by assigning damping parameters ζ_j to each mode, where $\zeta_j = c_1 j^2 + c_2 j^{1/2}$. This model is based on correlations developed by Matveev [19] and has been used in similar thermoacoustic systems [18,20]. It represents acoustic energy losses due to radiation from the open ends and dissipation in the acoustic viscous and thermal boundary layers at the duct walls. The dimensionless energy equation is then multiplied by $\sin(k\pi x)$ and integrated over the domain $x = [0, 1]$, thus reducing it to an ordinary differential equation for each mode j, as follows:

$$\frac{d}{dt}\left(\frac{\dot{\eta}_j}{j\pi}\right) + j\pi\eta_j + \zeta_j\left(\frac{\dot{\eta}_j}{j\pi}\right) + 2\beta\sin(j\pi x_f) = 0 \tag{8}$$

which is integrated by direct time-marching from $t = 0$ using a fourth order Runge–Kutta algorithm.

3 Model for the Premixed Flame

The flame is described by a kinematic model using a level set approach, also known as the G-equation model. Although this model is less complex than real premixed flames, it has been shown that it captures the major nonlinearities in premixed flame dynamics [12,15] and is used widely in low-order models of thermoacoustic systems with premixed flames [11,12,15,21,22].

The principal assumptions of the model are [23]: (i) the flame is a thin surface separating unburnt reactants from burnt products, and (ii) the flow is parallel along the axial direction with no transverse velocities. Assumption (i) allows for the flame to be tracked using the G-equation (in two dimensions), as follows:

$$\frac{\partial G}{\partial \tilde{t}} + \tilde{U}\frac{\partial G}{\partial \tilde{x}} + \tilde{V}\frac{\partial G}{\partial \tilde{y}} = s_L\sqrt{\left(\frac{\partial G}{\partial \tilde{x}}\right)^2 + \left(\frac{\partial G}{\partial \tilde{y}}\right)^2} \tag{9}$$

where tildes denote dimensional values and $G(x,y,t)$ is a time-varying function that takes negative values at points in the unburnt gas, positive values at points in the burnt gas, and zero at points that lie on the flame surface. Here, $\tilde{U}$ and $\tilde{V}$ are the instantaneous total velocities along the x and y directions. The flame speed s_L is a function of the local equivalence ratio, however, we only consider the dynamics of velocity perturbations imposed on fully premixed flames, ignoring flame-stretch effects. Hence, the equivalence ratio and flame speed are assumed to be uniform throughout the flow. Assumption (ii) allows for the velocity field to be independently specified, neglecting the coupling between the flow-field and flame surface evolution, and is the major simplifying assumption of this reduced order modeling approach. Equation (9) can be rewritten in terms of the nondimensional parameters $x^* = \tilde{x}/L_f$, $y^* = \tilde{y}/R$, $u^* = \tilde{U}/\tilde{u}_0$, $v^* = \tilde{V}/\tilde{u}_0$, and $t^* = \tilde{t}\tilde{u}_0/L_f$ as

$$\frac{\partial G}{\partial t^*} + u^*\frac{\partial G}{\partial x^*} + \beta_f v^*\frac{\partial G}{\partial y^*} = \left(\frac{s_L}{\tilde{u}_0}\right)\sqrt{\left(\frac{\partial G}{\partial x^*}\right)^2 + \beta_f^2\left(\frac{\partial G}{\partial y^*}\right)^2} \tag{10}$$

where L_f is the nominal flame height, i.e., the height of the steady flame ignoring stretch effects, R is the half-width of the burner, and β_f is the flame aspect ratio L_f/R.

The nonlinearity in heat release fluctuations is more pronounced in short flames compared to long flames [15]. For a given mean velocity, the shortest flame is that which has the greatest flame speed. In order to allow for a greater degree of nonlinearity, ϕ is chosen such that s_L is maximized. For the ϕ-dependence used in this paper [24], $\phi = 1.06$ maximizes s_L to 0.42 m/s and this flame speed is used throughout this study.

Several perturbation velocity models have been proposed. Early studies have used a uniform axial velocity perturbation [25,26]. However, it was shown by Baillot et al. [27,28] that the shear layers at the slot lips roll up into vortices that advect downstream and distort the flame surface. This was modeled as a convective wave that propagates through the velocity field of a vibrating flame by Schuller et al. [22] in order to calculate the flame transfer function (FTF). This model predicted the gain and phase of the FTF over a range of Strouhal numbers with reasonable accuracy. Within the flame domain, if the divergence-free assumption is used for the hydrodynamics, the continuity equation can be solved to find the transverse velocity perturbation field, given an axial velocity perturbation field. This was done by Preetham et al. [22] and, more recently, by Cuquel et al. [29], who have also derived analytical flame transfer functions with both axial and transverse velocity perturbations. However, Preetham et al. [22] show that the differences between transfer functions calculated using a purely axial velocity perturbation field and one with both axial and transverse perturbations are negligible. Hence, for the sake of simplicity, a purely axial convective wave velocity perturbation model is adopted in this paper. The nondimensionalized velocity field is specified as a harmonically oscillating traveling wave as

$$u^* = 1 + \varepsilon\cos(2\pi\,\mathrm{St}(Kx^* - t^*)) \tag{11}$$

where $\varepsilon = \tilde{u}/\tilde{u}_0$ is the nondimensional velocity perturbation, $\mathrm{St} = fL_f/\tilde{u}_0$ is the excitation Strouhal number, and $K = \tilde{u}_0/\tilde{u}_c$ is the ratio of the mean velocity to the disturbance convection speed (phase speed of velocity disturbances). Typically K is assumed to be equal to 1, i.e., the phase speed is assumed to equal the mean flow velocity. As seen in experiments [27,30], however, the phase speed of the velocity disturbances depends on a variety of factors such as the forcing frequency, amplitude, shear layer characteristics, temperature, and density changes across the flame surface, burner geometry, etc. In order to capture the dependence of the phase speed on the previously mentioned parameters, K is retained as a parameter in the model and the implications of the value of K on the nonlinear behavior of the system is described in Sec. 6.

Equation (10) is numerically solved using a weighted essentially nonoscillatory (WENO) fifth order scheme [31] for spatial discretization with a third order total variation diminishing (TVD) Runge–Kutta scheme [32] for time integration. The nondimensionalized spatial and temporal resolution in all the simulations are 5×10^{-3} and 5×10^{-4}, respectively, with a uniform mesh spacing in both spatial directions. The local level set method is used to achieve a significant reduction in the computational cost associated with these computations [33]. These computations are performed within the framework of LSGEN2D, a general level set method solver, which was developed by the second author [23,34].

Figure 2 shows instantaneous flame images over one forcing cycle. Note the formation of sharp cusps towards the products, a distinct characteristic of premixed flames seen in experiments [26,27,35].

For a premixed flame, the heat release rate can be written as an integral of local heat release rate contributions over the flame surface, which can be expressed in terms of G as an integral over the whole domain [36] as follows:

$$q(t) = \int_D \rho s_L(\phi) h_R(\phi) |\nabla G| \delta(G) dx^* dy^* \tag{12}$$

where $\delta(G)$ is the Dirac-delta function and $h_R(\phi)$ is the heat of reaction. The preceding integral can be numerically evaluated using the formulation by Smereka [36]. Note that, for fully premixed flames with constant flame speed, heat release rate oscillations are only due to flame surface area fluctuations induced by velocity perturbations that distort the flame surface.

4 Integral Criteria for Limit Cycles: Amplitudes and Stability

The Rayleigh criterion is a well-known and widely used criterion in thermoacoustics to determine whether acoustic disturbances in a system grow in magnitude. In the generalized form, as stated by Morgans and Dowling [37], an acoustic mode grows in amplitude if the energy gain from combustion exceeds the energy losses from the boundaries averaged over a period of the acoustic

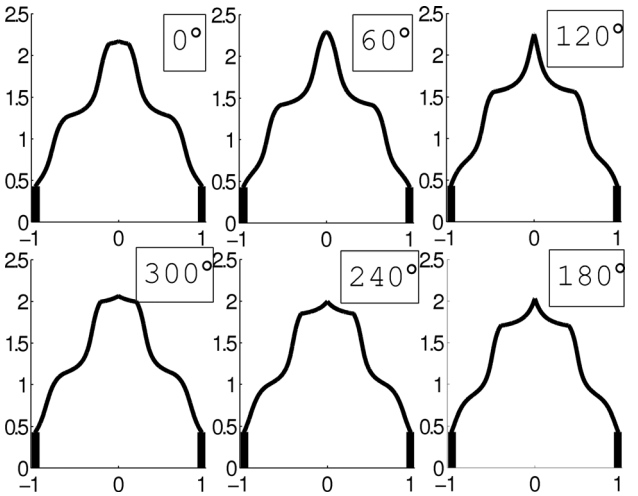

Fig. 2 Instantaneous images of the flame during one forcing cycle; $\phi = 1.06$, $\beta_f = 2.14$, $\varepsilon = 0.25$, $\mathrm{St} = 1$, and $K = 2.5$. The thick black line represents the slot burner and the thin black curve is the flame surface. Note the formation of sharp cusps towards the products, which is a distinct characteristic of premixed flames seen in experiments [26,27,35].

oscillation. As noted by Rayleigh, the phase difference between the pressure and heat release rate is crucial in determining the acoustic energy change over a cycle [38]. The Rayleigh criterion, however, does not provide the amplitude of limit cycle oscillations.

The purpose of this section is to propose a method to determine the amplitude of periodic oscillations in simple thermoacoustic systems and to identify their stability. The method used here is similar to the method of averaging developed by Culick [3,4]. In order to simplify the analysis, we consider only the fundamental acoustic mode. This simplification is reasonable because: (i) higher modes tend to be strongly damped, and (ii) the flame response at higher harmonics is usually small. While the single-mode assumption precludes interactions between modes, it allows one to derive analytical results that provide insight into the nonlinear dynamics of simple thermoacoustic systems.

The acoustic velocity perturbation is written as

$$\tilde{u} = \varepsilon \tilde{u}_0 \cos(\omega \tilde{t} + \varphi) \cos\left(\frac{\pi \tilde{x}}{L_0}\right) \tag{13}$$

Solving for the acoustic pressure perturbation using the dimensional momentum (Eq. (1)) with the appropriate boundary conditions (Eq. (6)) yields

$$\tilde{p} = \varepsilon \tilde{u}_0 \tilde{\rho}_0 \frac{\omega L_0}{\pi} \sin(\omega \tilde{t} + \varphi) \sin\left(\frac{\pi \tilde{x}}{L_0}\right) \tag{14}$$

The acoustic energy is written as the sum of potential and kinetic energies as

$$E \equiv \frac{1}{2}\left(\frac{\tilde{p}^2}{\tilde{\rho}_0 \tilde{c}_0^2} + \tilde{\rho}_0 \tilde{u}^2\right) \tag{15}$$

When a thermoacoustic system reaches a limit cycle, the rate of change of the acoustic energy integrated over the domain and over one cycle of oscillation is zero, i.e.,

$$\oint \int_D \frac{\partial E}{\partial \tilde{t}} \mathrm{d}\tilde{x}\mathrm{d}\tilde{t} = \oint \int_D \left(\frac{\tilde{p}}{\tilde{\rho}_0 \tilde{c}_0^2}\frac{\partial \tilde{p}}{\partial \tilde{t}} + \tilde{\rho}_0 \tilde{u}\frac{\partial \tilde{u}}{\partial \tilde{t}}\right)\mathrm{d}\tilde{x}\mathrm{d}\tilde{t} = 0 \tag{16}$$

Using the dimensional energy (Eq. (2)) for $\partial \tilde{p}/\partial t$, this reduces to

$$\oint \int_D \left(\frac{(\gamma - 1)\tilde{p}\tilde{\dot{Q}}\tilde{\delta}(\tilde{x} - \tilde{x}_f)}{\tilde{\rho}_0 \tilde{c}_0^2} - \frac{\zeta \tilde{p}^2}{\tilde{\rho}_0 \tilde{c}_0 L_0}\right)\mathrm{d}\tilde{x}\mathrm{d}\tilde{t} = 0 \tag{17}$$

Using Eqs. (13) and (14) and integrating over the domain $\tilde{x} = [0, L_0]$, recollecting that $\tilde{x}_f$ is the flame position, yields

$$\oint \left(2\beta \dot{Q} \sin(\omega \tilde{t} + \varphi) \sin\left(\frac{\pi \tilde{x}_f}{L_0}\right) - \frac{\omega L_0}{\pi \tilde{c}_0} \zeta \varepsilon \sin^2(\omega \tilde{t} + \varphi)\right)\mathrm{d}\tilde{t} = 0 \tag{18}$$

In general, the heat release rate perturbation is a nonlinear function of $\tilde{u}$ and contains higher harmonics of the fundamental frequency ω. It can be written as a Fourier series

$$\dot{Q} = \sum_{k=1}^{\infty} q_k \cos(k\omega \tilde{t} + \varphi_k) \tag{19}$$

If the phase difference between the terms in the expansion of $\dot{Q}$ and the acoustic velocity perturbation are written as $\Delta\varphi_k \equiv k\varphi - \varphi_k$ and the orthogonality of the Fourier series is used, the cyclic integral (Eq. (18)) reduces to

$$\oint (\Psi_{\mathrm{driv}} - \Psi_{\mathrm{damp}}) \sin^2(\omega \tilde{t} + \varphi)\mathrm{d}\tilde{t} = 0 \tag{20}$$

$$\Psi_{\mathrm{driv}} \equiv 2\beta \sin\left(\frac{\pi \tilde{x}_f}{L_0}\right) q_1 \sin(\Delta\varphi_1), \quad \Psi_{\mathrm{damp}} \equiv \frac{\omega L_0}{\pi \tilde{c}_0}\zeta\varepsilon \tag{21}$$

In the preceding equation, the driving and damping terms, Ψ_{driv} and Ψ_{damp}, are constant on a limit cycle. Hence, for Eq. (20) to be true, the driving and damping terms must be equal, i.e., $\Psi_{\mathrm{driv}} = \Psi_{\mathrm{damp}}$, or

$$2\beta \sin\left(\frac{\pi \tilde{x}_f}{L_0}\right) q_1 \sin(\Delta\varphi_1) = \frac{\omega L_0}{\pi \tilde{c}_0}\zeta\varepsilon_s \tag{22}$$

This equation shows that when a thermoacoustic system reaches a limit cycle, the gain of the velocity-coupled FDF q_1/ε and the phase of the velocity-coupled FDF $\Delta\varphi_1$ are explicitly related to the damping factor ζ. With measured or computed FDFs, the preceding equation can be used to find the amplitude of acoustic velocity perturbations, ε_s on the limit cycles. This equation also shows that for a single-mode system, over one cycle of the oscillation, only the fundamental of the heat release rate contributes to the limit cycle amplitude.

The stability of limit cycles is obtained by calculating the gradient of the left hand side of Eq. (20) with respect to ε, i.e.,

$$\left[\frac{\partial}{\partial \varepsilon}\oint (\Psi_{\mathrm{driv}} - \Psi_{\mathrm{damp}})\sin^2(\omega \tilde{t} + \varphi)\mathrm{d}\tilde{t}\right]_{\varepsilon_s} < 0 \tag{23}$$

implies that the limit cycle is stable.

5 Linear and Nonlinear Flame Response

The linear and nonlinear velocity-coupled response of premixed flames has been extensively studied [15,16,21,22,35,39]. The configuration investigated here, however, is a 2-D slot-stabilized flame, which has different response characteristics and it is useful to highlight the main features of its FDF. Figure 3 shows the gain and phase of the FDF of the heat release rate response to velocity perturbations. As noted by several researchers in the past, the gain at low frequencies tends to unity, the phase at low frequencies is zero, and the low frequency behavior is largely linear [40]. The phase increases with the St, which is characteristic of systems with a time-delay.

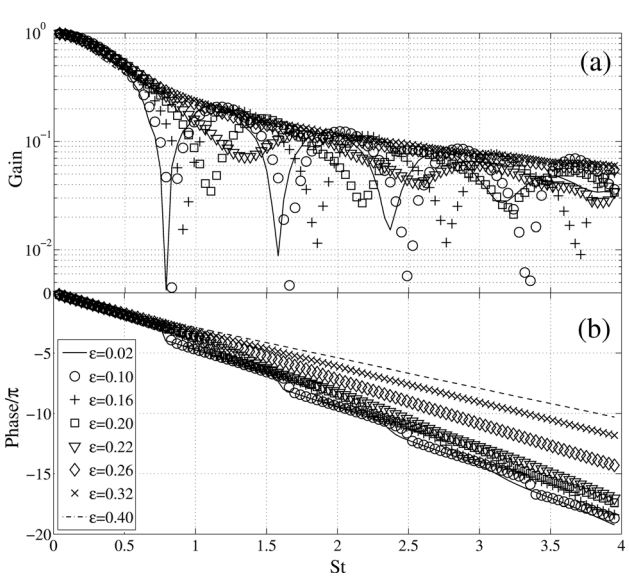

Fig. 3 Flame describing function FDF$(\omega,\varepsilon) = \tilde{\dot{Q}}'/\tilde{\dot{Q}}_0/\tilde{u}'/\tilde{u}_0$: (*a*) gain, and (*b*) phase $K = 2.5$, $\beta_f = 2.14$, $\phi = 1.06$

The FDF has zeros due to the destructive interference between disturbances created on the flame surface from flow nonuniformity and the flame anchoring boundary condition [22]. When these zeros are located close to the imaginary axis in the complex plane, they result in a sharp decrease in the gain and a phase jump of π across the St at which they are located; for example, at St $= 0.8, 1.6, 2.4, \ldots$. However, as the forcing amplitude increases, all zeros move to a higher Strouhal number. This suggests that the time-delay between the heat release rate and velocity perturbations decreases, which is due to the decrease in the mean flame height as the amplitude increases. Second, as the forcing amplitude increases, the zeros move further away from the imaginary axis in the complex plane. Hence the decrease in gain is less dramatic in the vicinity of the zeros and the phase decrease of π is spread over a wider range of Strouhal number. At large forcing amplitudes, the zeros are very far away from the imaginary axis. Hence, the gain and phase are smooth and monotonically decrease with frequency.

The amplitude-dependent behavior of the zeros results in a significant gain and phase variation of the FDF. Crucially, at a given St, the amplitude dependence of the gain is not monotonic and saturation does not always occur. Indeed, at some frequencies, the gain increases as the forcing amplitude increases. Preetham et al. proposed that the amplitude dependence of the gain determines whether a system exhibits subcritical bifurcations [22]. This rests on the assumption, however, that the FDF phase remains constant at all amplitudes. This is not the case for the flame investigated in this article. At a given St, the phase difference decreases as the amplitude increases and the decrease is most dramatic when a zero crosses that particular St. Section 6 shows how the combined effect of the amplitude-dependence of the gain and phase impacts the nonlinear dynamics of these systems.

Finally, it is important to note that when K, the ratio of the mean velocity $\tilde{u}_0$ to the disturbance phase speed $\tilde{u}_c$ is assumed to be zero (i.e., a spatially uniform disturbance) or one (i.e., the disturbance phase speed equals the mean flow velocity), the FDF does not exhibit the features previously discussed. The nonlinearities of the flame response for these special cases result in a monotonic decrease in the gain and a negligible change in the phase, as the amplitude increases [15,22]. The effect of K on the nonlinear dynamics of this system will be highlighted in Sec. 6.

6 Cyclic Integral of Rate of Change of Energy (CIRCE) Diagrams

Using the integral criterion derived in Sec. 4, a stability diagram of single-mode thermoacoustic systems can be constructed, as shown in Fig. 4. This is a diagram of the cyclic integral of rate of change of energy (CIRCE) as a function of the nondimensional velocity perturbation amplitude (vertical axis), across different single-mode systems of varying nondimensional resonant frequencies (horizontal axis). Note that each nondimensional frequency corresponds to a thermoacoustic system with a different duct length. Hence, for a given system, the diagram is to be interpreted by moving along the amplitude axis (vertical axis) at the frequency that corresponds to the fundamental mode of that system. Each frame of Fig. 4 corresponds to a different value of K—the ratio of the mean velocity to the disturbance phase speed.

The gray-scale is such that regions where driving exceeds damping are light, while regions where damping exceeds driving are dark. The boundaries between light and dark regions, marked by the black curves, are locations where driving and damping are exactly equal and, hence, they correspond to the limit cycles of the system. The vertical dashed lines in each frame represent the scenarios examined later, in terms of the number of limit cycles that exist and their stability. Furthermore, the criterion in Eq. (23) is used to infer the stability of these limit cycles.

Before investigating the different scenarios in detail, it is useful to note that the differences between Figs. 4(*a*)–4(*c*) illustrate the strong influence of K, the ratio of the mean velocity to the disturbance phase speed, on the nonlinear behavior of the system. The shapes of the limit cycle contours and the number of limit cycles that exist for a particular system (i.e., for a particular nondimensional frequency) are direct manifestations of the gain and phase variation of the corresponding FDFs. The amplitude-dependence of the phase of the FDF for the $K = 1$ case is negligible, whereas the gain saturates at high amplitudes. Hence, only a single intersection of the driving and damping curves is possible for linearly unstable systems and, at most, one limit cycle exists at a given frequency, as seen in Fig. 4(*a*). For the $K = 2.5$ case, however, the gain is not monotonic and the phase changes by several multiples of π, as the amplitude increases. Hence, as the amplitude increases, the driving curve has several sign changes and multiple intersections with the damping line are possible, resulting in several limit cycles, as seen in Fig. 4(*c*). The gain and phase of the FDF of the $K = 1.5$ case show a weaker amplitude-dependence compared to the $K = 2.5$ case; hence, it has fewer limit cycles at a given system frequency. As discussed in Sec. 5, the gain and phase variation is due to the behavior of the zeros of the FDF and their influence is clearly seen in these CIRCE diagrams.

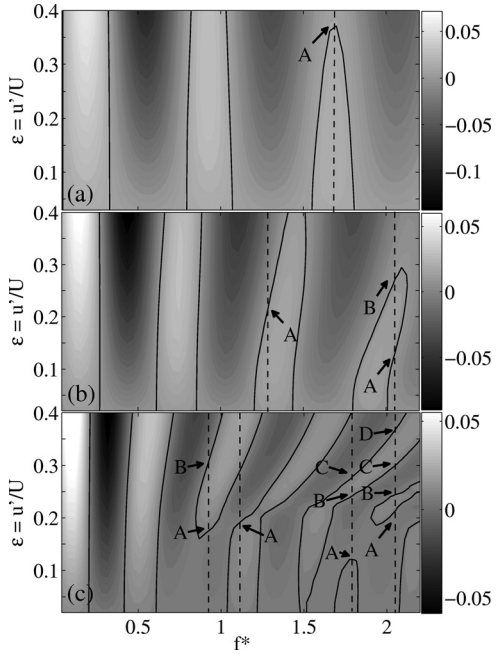

Fig. 4 CIRCE diagram: driving (Ψ_{driv}) – damping (Ψ_{damp}) as a function of amplitude ε for thermoacoustic systems with different fundamental frequencies f^*: (*a*) $K = 1.0$, (b) $K = 1.5$, and (*c*) $K = 2.5$

Figures 5 and 6 are slices of the CIRCE diagram that depict the four different scenarios marked by the dashed lines in Fig. 4(*c*). In these figures, the solid line represents the driving term Ψ_{driv}, while the dashed line represents the damping term Ψ_{damp}. The complicated amplitude-dependence of Ψ_{driv} is due to the amplitude-dependence of the gain and phase of the FDF and will be discussed in detail later.

Figure 5(*a*) shows a system that is linearly unstable about the fixed point because driving exceeds damping at small amplitudes. At point-A, where the driving and damping balance each other, a limit cycle is established. Furthermore, the gradient of the CIRCE (see Eq. (23)) at point-A is negative; therefore, this limit cycle is stable. This situation corresponds to a monostable state. In terms of a control parameter such as βq_1, this corresponds to a supercritical bifurcation.

On the contrary, Fig. 5(*b*) shows a system that is linearly stable about the fixed point. Indeed, the so-called driving term is negative in the linear limit due to the sign of the phase difference, i.e., $\sin(\Delta\varphi_1) < 0$ for small ε. However, as the amplitude increases, changes in the driving term result in two intersections with the

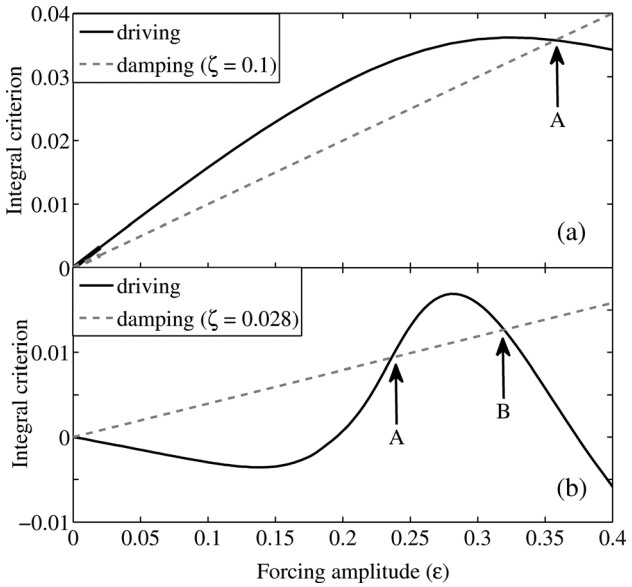

Fig. 5 CIRCE for thermoacoustic systems with different fundamental frequencies (duct lengths): $K = 2.5$, $\phi = 1.06$, and $\beta_f = 2.14$. (*a*) Slice of Fig. 4(*c*) at $f^* = 0.4$: A is the stable limit cycle, and (*b*) slice of Fig. 4(*c*) at $f^* = 1.0$; A is the unstable limit cycle, and B is the stable limit cycle.

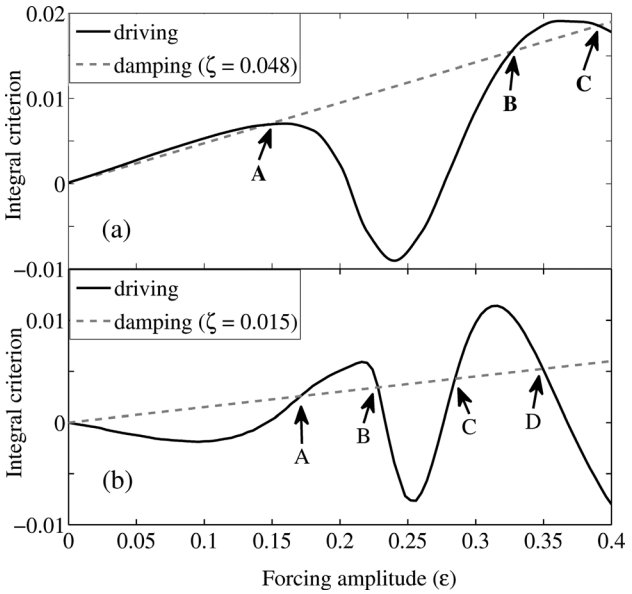

Fig. 6 CIRCE for thermoacoustic systems with different fundamental frequencies (duct lengths): $K = 2.5$, $\phi = 1.06$, and $\beta_f = 2.14$. (*a*) Slice of Fig. 4(*c*) at $f^* = 1.2$: A and C are the stable limit cycles, B is the unstable limit cycle, and (*b*) slice of Fig. 4(*c*) at $f^* = 1.8$: A and C are the unstable limit cycles, B and D are the stable limit cycles.

damping line at points A and B, which are an unstable and a stable limit cycle, respectively. If the system in its linearly stable state is given an excitation with amplitude greater than the amplitude of state-A, oscillations in the system will grow until the system reaches state-B. This phenomenon is called triggering. In a single-mode thermoacoustic system, the minimum amplitude of an excitation that can cause triggering is the amplitude at point-A. For this minimum amplitude excitation to be successful in triggering the system, however, the excitation has to be given in the right direction. For example, in the case of velocity-coupled oscillations of a premixed flame, the velocity excitation has to be given when the flame shape is most receptive to this excitation. In a system with several modes, however, it has been shown that triggering can occur, due to nonnormal transient growth, at amplitudes smaller than that of the unstable limit cycle [20]. The situation depicted in Fig. 5(*b*) corresponds to a bistable state. In terms of a control parameter such as βq_1, this corresponds to a subcritical bifurcation.

The systems shown in Figs. 6(*a*) and 6(*b*) have a similar linear behavior to those of Figs. 5(*a*) and 5(*b*), but have a more complex nonlinear behavior because the gain and phase, at high St, vary greatly as the amplitude increases. Using the same reasoning as before, Fig. 6(*a*) shows that the system has stable limit cycles at A and C and an unstable limit cycle at B. From the stable oscillating state at A, the system can be triggered into large amplitude oscillations with an excitation of amplitude greater than that of point-B. This situation corresponds to a bistable state. In terms of a control parameter such as βq_1, this corresponds to a supercritical bifurcation followed by two fold bifurcations. As mentioned in Ref. [9], a system must have either a subcritical bifurcation or a supercritical bifurcation followed by fold bifurcations in order to be susceptible to triggering.

Finally, Fig. 6(*b*) shows a system that is linearly stable, has two unstable limit cycles (A and C), and two stable limit cycles (B and D). An excitation with amplitude greater than that of A, but less than that of C, will eventually lead to stable oscillations at B. An excitation with amplitude greater than that of C, however, will lead to stable oscillations at D. As in Fig. 6(*a*), the system can be triggered from one stable limit cycle to another by a suitably large excitation. This situation corresponds to a tristable state. In terms of a control parameter such as βq_1, this corresponds to a subcritical bifurcation followed by two fold bifurcations.

This wide range of behavior in Figs. 5 and 6 can be explained by examining the amplitude-dependence of the gain and phase in Fig. 3. First, the supercritical bifurcation seen in Fig. 5(*a*) at $\mathrm{St} = 0.4$ is because the gain decreases as the forcing amplitude increases, while the phase remains fairly constant. This is the most commonly described route to a limit cycle in thermoacoustic systems. Second, the subcritical bifurcation seen in Fig. 5(*b*) at $\mathrm{St} = 1.0$ is because the phase changes significantly as the amplitude increases. Figure 7(*a*) shows the fundamental of the heat release rate q_1, Fig. 7(*b*) shows the phase difference between the fundamental of heat release rate and velocity $\Delta\varphi_1$, and Fig. 7(*c*) shows $\sin(\Delta\varphi_1)$ at $\mathrm{St} = 1.03$. Note that $\sin(\Delta\varphi_1)$ is negative at low amplitudes (gray shaded area) but changes sign at around $\varepsilon = 0.2$. Since $\sin(\Delta\varphi_1)$ is a factor in the driving term, it is clear that the driving becomes positive at a finite amplitude, reaches a peak, and then decreases at high amplitudes, as seen in Fig. 5(*b*). Depending on the value of the damping factor ζ, an unstable and a stable limit cycle can exist between $\varepsilon = 0.2$ and $\varepsilon = 0.38$. A subcritical bifurcation is also possible when the amplitude-dependence of the gain is such that it increases as the forcing amplitude increases, followed by saturation at high amplitudes. This behavior is most likely to be seen at a linear zero of the FDF, for example, at $\mathrm{St} = 0.8$. Figure 7(*d*) shows q_1 versus the forcing amplitude at $\mathrm{St} = 0.8$. For this frequency, the phase difference remains constant as the amplitude increases. Hence, this corresponds to a driving curve with an inflection point, which permits two limit cycles at finite amplitudes. The preceding two examples are special cases, where the amplitude-dependence of either the gain or the phase leads to a subcritical bifurcation. In most cases, however, it is the combined effect of the gain and the phase which results in the driving curve intersecting the damping line twice, which, for a linearly stable system, represents a subcritical bifurcation. Finally, at high frequencies, the changes in the gain are small, whereas the changes in phase are large. Indeed, the dramatic changes seen in the driving term in Figs. 6(*a*) and 6(*b*) and the multiple intersections with the damping line are due to the large variation in phase, as amplitude increases, at high St.

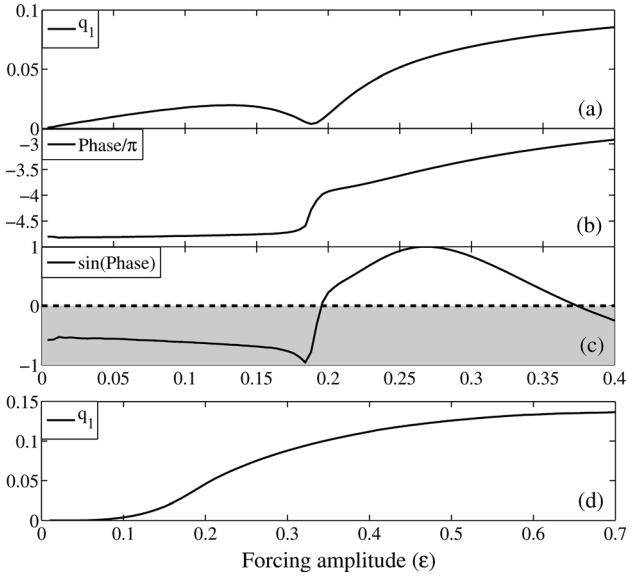

Fig. 7 Amplitude-dependence of the fundamental of heat release rate oscillations and the phase between the heat release rate and velocity perturbations: $K = 2.5$, $\phi = 1.06$, and $\beta_f = 2.14$. (*a*) q_1 at St = 1.0, (*b*) $\Delta\varphi_1$ at St = 1.0, and (*c*) $sin(\Delta\varphi_1)$ at St = 1.0. The gray shaded area shows regions where driving is negative, while white shows where it is positive. (*d*) q_1 at St = 0.8.

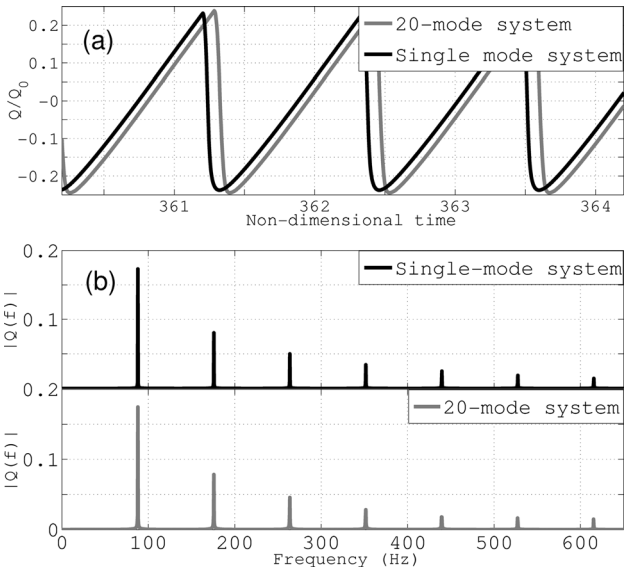

Fig. 9 Nonlinear heat release rate oscillations in thermoacoustic systems with one mode and twenty modes: $f^* = 0.87$, $K = 1.5$, $\beta_f = 2.14$, $\phi = 1.06$, and $\zeta = 0.05$ ($c_1 = 0.03$, $c_2 = 0.02$). (*a*) Time trace of the heat release rate (phase-shifted to avoid overlap of figures), and (*b*) Fourier transforms of the heat release rate.

7 Time Domain Simulations

The analyses in the previous sections were based on the analytical results for a single-mode system with amplitude-dependent information derived from the FDF. It is useful to compare these results with the time-domain calculations of self-excited oscillations to verify the accuracy of the frequency-domain predictions.

Figure 8 shows the time domain calculations of self-excited thermoacoustic systems with one Galerkin mode and twenty Galerkin modes. Both of these systems have a nondimensional fundamental frequency of $f^* = 0.87$, which, for a duct of length L_0 of 1.954 m and a flame length, L_f of 1×10^{-2} m, corresponds to a dimensional fundamental frequency of 87 Hz. These systems are linearly unstable and have supercritical bifurcations. Figure 8(*a*) shows that the two systems reach limit cycles of different amplitudes. Figure 8(*b*) shows that the higher Galerkin modes contain approximately ten percent of the total energy of the system. The higher modes contribute to the increase in the amplitude of limit cycle oscillations seen in Fig. 8(*a*).

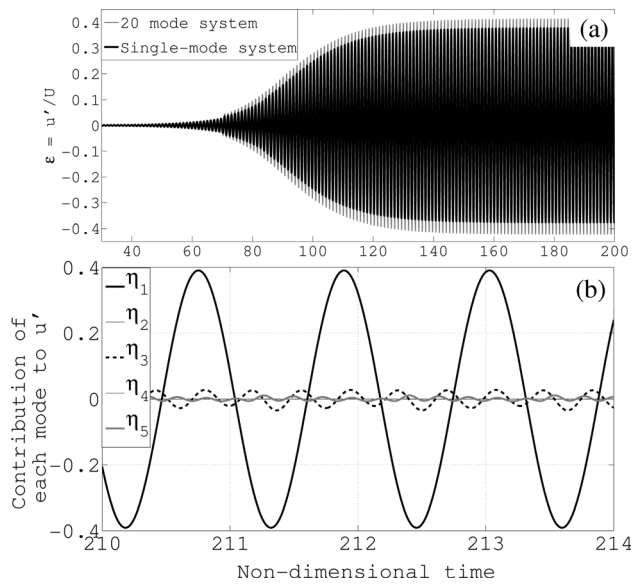

Fig. 8 Time domain calculations for self-excited thermoacoustic systems with one mode and twenty modes: $f^* = 0.87$, $K = 1.5$, $\beta_f = 2.14$, $\phi = 1.06$, and $\zeta = 0.05$ ($c_1 = 0.03$, $c_2 = 0.02$). (*a*) Time trace of the acoustic velocity perturbations at the flame location x_f, and (*b*) time trace of the contributions of the first five Galerkin modes to the acoustic velocity at the flame location x_f of the 20-mode system.

Figure 9(*a*) shows heat release rate oscillations, with one of the signals phase-shifted slightly in order to avoid overlap on the figure. The corresponding Fourier transforms are shown in Fig. 9(*b*). Note that the heat release rate signals are highly nonharmonic, with the first harmonic having a magnitude more than forty percent that of the fundamental. In the single-mode system, however, the higher harmonics of the heat release rate cannot interact with the velocity perturbations, as shown in Sec. 4. On the contrary, in the twenty-mode system, the higher harmonics of the heat release rate contribute to the dynamics by interacting with the higher acoustic velocity modes. For this reason, the twenty-mode system extracts more energy from the flame and transfers it to the acoustics, than does the single-mode system. As a result, the single-mode system reaches a limit cycle with $\varepsilon = 0.375$, while the twenty-mode system reaches a limit cycle with $\varepsilon = 0.415$.

The amplitude of oscillation predicted by the CIRCE criterion with information from the FDF, shown in Fig. 10, is $\varepsilon = 0.377$. Clearly, in spite of a fairly high degree of nonlinearity in the heat release signal, very good agreement is obtained between the single-mode time domain and frequency domain results. An important point to note is that close agreement is to be expected when time-domain simulations of a single-mode system are compared against results from the criterion derived in Sec. 4, because only the fundamental modes of the heat release rate and acoustic velocity can interact, as shown in Sec. 4. For the twenty-mode system, however, the effect of the higher modes on the system dynamics is not negligible and the twenty-mode system has a limit cycle amplitude that is larger than that of the single-mode system.

At the operating condition of the example previously discussed, the difference in the limit cycle amplitude between the single-mode and twenty-mode systems is about ten percent. There can,

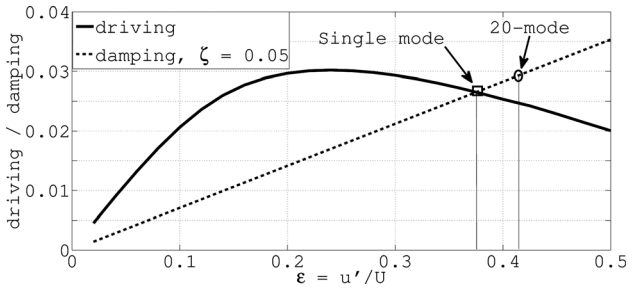

Fig. 10 CIRCE diagram: the intersection of driving and damping curves represents the frequency domain prediction for the limit cycle amplitude. Time-domain limit cycle locations are marked by symbols: $f^* = 0.87$, $K = 1.5$, $\beta_f = 2.14$, $\phi = 1.06$, and $\zeta = 0.05$ ($c_1 = 0.03$, $c_2 = 0.02$).

however, be operating conditions where large discrepancies exist between the single-mode and multimode systems. Such discrepancies would indicate that interactions between the higher modes play a crucial role in the system dynamics. A detailed analysis of this is beyond the scope of this paper and will be the subject of future investigations.

8 Conclusions

This paper examines the nonlinear thermoacoustic phenomena in self-excited oscillations of a simple premixed flame in a tube. The flame is modeled using a nonlinear kinematic model based on the G-equation, while the acoustics are governed by linearized momentum and energy equations. Assuming the existence of limit cycles, integral criteria are derived for a single mode thermoacoustic system to estimate the amplitudes of limit cycles and their stability. Using open-loop forced simulations, the sinusoidal flame describing function (FDF) is calculated. The FDF has zeros because of the interactions between the two types of flame front disturbances characteristic of anchored premixed flames with nonuniform velocity fields. The amplitude-dependence of the gain and phase of the FDF is shown to be related to the amplitude-dependence of the zeros of the FDF. The integral criteria are used with the amplitude-dependence of the gain and phase of the FDF to construct cyclic integral of rate of change of energy (CIRCE) diagrams that show precisely when a thermoacoustic system is monostable, bistable, or tristable. These diagrams are also used to show the types of bifurcation seen in such systems and to find the minimum amplitude of excitation required to trigger a single-mode thermoacoustic system into limit cycle oscillations.

The choice of velocity model and the phase speed of convective disturbances are shown to be crucial for the prediction of nonlinear dynamics of thermoacoustic systems. When K, the ratio of the mean velocity to the phase speed of convective disturbances, is assumed to be zero or one, which are the most commonly made assumptions, the system can have only one stable state. For other values of K, several limit cycles exist and the system has combinations of fold bifurcation and either supercritical or subcritical Hopf bifurcations, depending on the operating condition.

Previous studies have highlighted the influence of the amplitude dependence of the FDF gain [22] or phase [16] on nonlinear behavior. In this paper, it is shown that there exist certain regions where either the gain or the phase is more influential, however, the combined effect of the gain and phase has to be considered to accurately predict nonlinear behavior.

Time domain simulations of the coupled thermoacoustic system are performed with a Galerkin discretization for acoustic pressure and velocity. Limit cycle calculations using a single mode, along with twenty modes, are compared against predictions from the CIRCE diagram. For the single mode system, the time domain calculations agree well with the frequency domain predictions. The heat release rate is highly nonharmonic, however, because there is only a single acoustic mode, this does not affect the limit cycle amplitude. For the twenty-mode system, however, the higher harmonics of the heat release rate interact with those of the acoustic velocity, resulting in a larger limit cycle amplitude. Multimode simulations show that, in some situations, the contribution from higher harmonics to the nonlinear dynamics can be significant and must be considered for an accurate and comprehensive analysis of thermoacoustic systems.

Acknowledgment

The first author would like to thank Simon Illingworth and Iain Waugh for helpful and enthusiastic discussions throughout the course of this project. This work was supported by the U.K. Engineering Physical and Sciences Research Council (EPSRC) and Rolls Royce Plc. The work of the second author was supported by the Deutsche Forschungsgemeinschaft (DFG) through the collaborative research center, SFB 686. The support is gratefully acknowledged.

Nomenclature

E = acoustic energy
f = forcing frequency
f^* = nondimensional natural frequency of the self-excited system ($c_0 L_f / 2\tilde{u}_0 L_0$)
G = level set function
h_R = heat of reaction per unit mass
K = ratio of mean velocity to disturbance convection speed, $\tilde{u}_0/\tilde{u}_c$
p = pressure
$\dot{Q}$ = heat release rate
R = half-width of the burner
s_L = laminar flame speed
St = Strouhal number, $fL_f/\tilde{u}_0$
u = velocity

Greek Symbols

β_f = flame aspect ratio, L_f/R
γ = ratio of specific heats
δ = Dirac-delta function
ε = velocity perturbation amplitude
ζ = damping coefficient
ρ = density
ϕ = equivalence ratio
φ = phase
ω = angular frequency

References

[1] Lieuwen, T. C. and Yang, V., 2005, "Combustion Instabilities in Gas Turbine Engines," *Progress in Astronautics and Aeronautics*, Vol. 210, AIAA, Reston, Va.
[2] Zinn, B. T. and Lores, M. E., 1972, "Application of the Galerkin Methods in the Solution of Nonlinear Axial Combustion Instability Problems in Liquid Rockets," Combust. Sci. Technol., **4**, pp. 269–278.
[3] Culick, F. E. C., 1976, "Nonlinear Behaviour of Acoustic Waves in Combustion Chambers—Part 1," Acta Astronaut., **3**, pp. 715–734.
[4] Culick, F. E. C., 1976, "Nonlinear Behaviour of Acoustic Waves in Combustion Chambers—Part 2," Acta Astronaut., **3**, pp. 735–757.
[5] Yang, V. and Culick, F. E. C., 1990, "On the Existence and Stability of Limit Cycles for Transverse Acoustic Oscillations in a Cylindrical Combustion Chamber. I: Standing Modes," Combust. Sci. Technol., **72**(1), pp. 37–65.
[6] Yang, V., Kim, S. I., and Culick, F. E. C., 1990, "Triggering of Longitudinal Pressure Oscillations in Combustion Chambers. I: Nonlinear Gas Dynamics," Combust. Sci. Technol., **72**(4), pp. 183–214.
[7] Baum, J. D., Levine, J. N., and Lovine, R. L., 1988, "Pulsed Instability in Rocket Motors: A Comparison Between Predictions and Experiment," J. Propul. Power, **4**(4), pp. 308–316.
[8] Wicker, J. M., Greene, W. D., Kim, S-I., and Yang, V., 1996, "Triggering of Longitudinal Pressure Oscillations in Combustion Chambers. I: Nonlinear Combustion Response," J. Propul. Power, **12**(6), pp. 1148–1158.
[9] Ananthkrishnan, N., Deo, S., and Culick, F. E. C., 2005, "Reduced-Order Modeling and Dynamics of Nonlinear Acoustic Waves in a Combustion Chamber," Combust. Sci. Technol., **177**(2), pp. 221–248.

[10] Poinsot, T., and Candel, S., 1988, "A Nonlinear Model for Ducted Flame Combustion Instabilities," Combust. Sci. Technol., **61**, pp. 121–153.
[11] Dowling, A. P., 1997, "Nonlinear Self-Excited Oscillations of a Ducted Flame," J. Fluid Mech., **346**, pp. 271–290.
[12] Dowling, A. P., 1999, "A Kinematic Model of a Ducted Flame," J. Fluid Mech., **394**, pp. 51–72.
[13] Stow, S. R., and Dowling, A. P., 2004, "Low-Order Modelling of Thermoacoustic Limit Cycles," ASME Turbo Expo, Vienna, Austria, June 14–17, ASME Paper No. GT2004-54245.
[14] Stow, S. R., and Dowling, A. P., 2008, "A Time-Domain Network Model for Nonlinear Thermoacoustic Oscillations," ASME Turbo Expo, Berlin, June 9–13, ASME Paper No. GT2008-50770.
[15] Lieuwen, T., 2005, "Nonlinear Kinematic Response of Premixed Flames to Harmonic Velocity Disturbances," Proc. Combust. Inst., **29**, pp. 99–105.
[16] Noiray, N., Durox, D., Schuller, T., and Candel, S. M., 2008, "A Unified Framework for Nonlinear Combustion Instability Analysis Based on the Flame Describing Function," J. Fluid Mech., **615**, pp. 139–167.
[17] Moeck, J. P., Bothien, M. R., Schimek, S., Lacarelle, A., and Paschereit, C. O., 2008, "Subcritical Thermoacoustic Instabilities in a Premixed Combustor," 14th AIAA/CEAS Aeroacoustics Conference, Vancouver, Canada, May 5–7, AIAA Paper No. 2008-2946.
[18] Subramanian, P., Gupta, V., Tulsyan, B., and Sujith, R. I., 2010, "Can Describing Function Technique Predict Bifurcations in Thermoacoustic Systems?," 16th AIAA/CEAS Aeroacoustics Conference, Stockholm, Sweden, June 7–9, AIAA Paper No. 2010-3860.
[19] Matveev, I., 2003, "Thermo-Acoustic Instabilities in the Rijke Tube: Experiments and Modeling," Ph.D. thesis, CalTech, Pasadena, CA.
[20] Juniper, M. P., 2011, "Triggering in the Horizontal Rijke Tube: Non-Normality, Transient Growth and Bypass Transition," J. Fluid Mech., **667**, pp. 272–308.
[21] Schuller, T., Durox, D., and Candel, S., 2003, "A Unified Model for the Prediction of Laminar Flame Transfer Functions: Comparisons Between Conical and *v*-Flame Dynamics," Combust. Flame, **134**, pp. 21–34.
[22] Preetham, Santosh, H., and Lieuwen, T., 2008, "Dynamics of Premixed Flames Forced by Harmonic Velocity Disturbances," J. Propul. Power, **24**(6), pp. 1390–1402.
[23] Shreekrishna, Hemchandra, S., and Lieuwen, T., 2010, "Premixed Flame Response to Equivalence Ratio Perturbations," Combust. Theory Model., **14**, pp. 681–714.
[24] Abu-Orf, G., and Cant, R. S., 1996, "Reaction Rate Modelling for Premixed Turbulent Methane-Air Flames," Proceedings of the Joint Meeting of Spanish, Portuguese, Swedish and British Sections of the Combustion Institute, Madeira, Portugal, April 1–4.
[25] Fleifil, M., Annaswamy, A., Ghoneim, Z., and Ghoneim, A., 1996, "Response of a Laminar Premixed Flame to Flow Oscillations: A Kinematic Model and Thermoacoustic Instability Results," Combust. Flame, **106**, pp. 487–510.
[26] Ducruix, S., Durox, D., and Candel, S., 2000, "Theoretical and Experimental Determination of the Transfer Function of a Laminar Premixed Flame," Proc. Combust. Inst., **28**, pp. 765–773.
[27] Baillot, F., Durox, D., and Prud'homme, R., 1992, "Experimental and Theoretical Study of a Premixed Vibrating Flame," Combust. Flame, **88**(2), pp. 149–168.
[28] Baillot, F., Bourehla, A., and Durox, D., 1996, "The Characteristics Method and Cusped Flame Fronts," Combust. Sci. Technol., **112**(1), pp. 327–350.
[29] Cuquel, A., Durox, D., and Schuller, T., 2011, "Theoretical and Experimental Determination of the Flame Transfer Function of Confined Premixed Conical Flames," 7th Mediterranean Combustion Symposium, Cagliari, Sardinia, Italy, September 11–15.
[30] Michalke, A., 1971, "Instability of a Compressible Circular Free Jet With Consideration of the Influence of the Jet Boundary Thickness," NASA Report No. TM 75190.
[31] Jiang, G.-S., and Peng, D., 2000, "Weighted ENO Schemes for Hamilton-Jacobi Equations," SIAM J. Sci. Comput. (USA), **6**, pp. 2126–2143.
[32] Gottlieb, S., and Shu, C., 1998, "Total Variation Diminishing Runge-Kutta Schemes," Math. Comput., **67**, pp. 73–85.
[33] Peng, D., Merriman, B., Osher, S., Zhao, H., and Kang, M., 1999, "A PDE-Based Fast Local Level Set Method," J. Comput. Phys., **155**(2), pp. 410–438.
[34] Hemchandra, S., 2009, "Dynamics of Turbulent Premixed Flames in Acoustic Fields," Ph.D. thesis, Georgia Institute of Technology, Atlanta, GA.
[35] Karimi, N., Brear, M. J., Jin, S.-H., and Monty, J. P., 2009, "Linear and Non-Linear Forced Response of a Conical, Ducted, Laminar Premixed Flame," Combust. Flame, **156**, pp. 2201–2212.
[36] Smereka, P., 2006, "The Numerical Approximation of a Delta Function With Application to Level Set Methods," J. Comput. Phys., **211**, pp. 77–90.
[37] Dowling, A. P., and Morgans, A. S., 2005, "Feedback Control of Combustion Oscillations," Ann. Rev. Fluid Mech., **37**, pp. 151–182.
[38] Rayleigh, J. W. S., 1945, *The Theory of Sound*, Vol. II, Dover, New York.
[39] Durox, D., Schuller, T., Noiray, N., and Candel, S., 2009, "Experimental Analysis of Nonlinear Flame Transfer Functions for Different Flame Geometries," Proc. Combust. Inst., **32**(1), pp. 1391–1398.
[40] Polifke, W., and Lawn, C., 2007, "On the Low-Frequency Limit of Flame Transfer Functions," Combust. Flame, **151**(3), pp. 437–451.